306 *Macromolecules* **2010**, *43*, 306–315
DOI: 10.1021/ma902132c

Macromolecules
ARTICLE

# Intercorrelation between Structural Ordering and Emission Properties in Photoconducting Polymers

**Silke Rathgeber,*,† Diogo Bastos de Toledo,‡ Eckhard Birckner,§ Harald Hoppe,⊥ and Daniel A. M. Egbe‖**

†*Johannes Gutenberg-University Mainz, Staudingerweg 7, 55128 Mainz, Germany,* ‡*Max Planck-Institute for Polymer Research Mainz, Ackermannweg 10, 55128 Mainz, Germany,* §*Institute of Physical Chemistry, Friedrich Schiller-University Jena, Lessingstrasse 10, 07743 Jena, Germany,* ⊥*Institute of Physics, Ilmenau University of Technology, Weimarer Strasse 32, 98693 Ilmenau, Germany, and* ‖*Linz Institute for Organic Solar Cells (LIOS), Johannes Kepler-University Linz, Altenbergerstrasse 69, 4040 Linz, Austria*

*Received September 28, 2009; Revised Manuscript Received November 2, 2009*

ABSTRACT: We investigated the structural properties of anthracene containing poly(*p*-phenylene−ethynylene)-*alt*-poly(*p*-phenylene−vinylene) polymers with general constitutional unit: (−Ph−C≡C−Anthr−C≡C−Ph−CH=CH−Ph−CH=CH−)$_n$ by means of wide-angle X-ray scattering and fluorescence spectroscopy. Interchain interactions were systematically modified by decorating the conjugated polymer backbone with linear or branched or combinations of linear and branched alkoxy side chains. Special emphasis is taken on an evaluation method for fiber scattering spectra that allows the deduction of important structural details of polymer materials with limited degree of order. These include positional correlations along the backbones, interlayer and $\pi-\pi$ stacking distances between different chains as well as a quantification of the degree of order in terms of number of lattice planes per domain. The polymers with all-linear side chains attached close to the anthracenylene−ethynylene unit (AnE) show a layered structure. In contrast attachment of branched side chains at the AnE unit leads to amorphous polymers. These structural differences are reflected in their photophysical properties, whereby the first group of polymers exhibit red-shifted emission as compared to the second group. The larger the $\pi-\pi$ stacking distance the more blue-shifted is the main emission band, but no clear correlation of the emission peak position is found with respect to the degree of order of the $\pi-\pi$ stacking in terms of number of $\pi-\pi$ lattice planes per domain. We also studied the effect of annealing on the *as synthesized* samples and observed structural transitions, which we attribute to side chain melting and backbone reorganization, respectively. Both transitions lead to enhanced structural order in the polymers which can be preserved during cooling the samples back to room temperatures. Once annealed, the polymers do not show significant structural changes over a wide temperature range, a property which we consider to be beneficial for photovoltaic applications.

## Introduction

The need and desire to develop cheap renewable energy sources have triggered worldwide intensive research for efficient, flexible, low cost and lightweight photovoltaic devices based on organic semiconducting materials.[1−4] Among the various types of organic photovoltaic cells, polymer−fullerene bulk heterojunction solar cells are by far the most successful with certified power conversion efficiencies around 6%.[5,6]

The photophysical and photovoltaic properties of polymer−fullerene active layers are to a large extent affected by the properties of the polymer phase. Conjugated polymers show, due to their semiflexible, liquid crystalline character supramolecular organization with complex thermotropic and lyotropic phase transitions.[7,8] The electronic and optical properties of conjugated polymers are strongly affected by their primary molecular structure (intramolecular functionality: $\pi$-conjugation) but also by supramolecular organization in particular by intermolecular $\pi-\pi$ interaction ($\pi-\pi$-stacking distance).[9] The photovoltaic and photophysical properties of polymer−fullerene active layers are in addition strongly affected by the extent of microphase separation.[10] The extent of microphase separation should be large enough to ensure sufficient charge separation. However, if the size of the microphase separated regions becomes too large, the donor−acceptor interfacial area is decreased and charge separation is hampered. Strong $\pi-\pi$ interaction (small $\pi-\pi$-stacking distance) supports unwanted strong phase separation of the active layer components.[11] In addition, it leads to a high tendency of excitonic self-quenching and other detrimental radiationless deactivation processes.[12] Thus, a detailed knowledge of the temperature dependent structural properties of conjugated polymers in particular of the $\pi-\pi$-stacking distance is essential for the understanding of the photovoltaic performance of polymer−fullerene solar cells.

The limited structural order in many crystallizing polymers leads to significant line broadening and the absence or at least fast decay of higher order scattering features. In addition scattering contributions from the amorphous side chains, from correlations along the backbone direction as well as from $\pi-\pi$-stacking will all contribute to the overall scattering intensity in a comparable $q$ region. Therefore, distinction of the different scattering contributions is often difficult or impossible from isotropic samples. Uniaxial extension into fibers is a well established method in polymer crystallography in order to separate the different contributions.[18] However, a low degree of order, not perfect alignment and the isotropic contribution of the amorphous side chains, quite often blurs the results and makes in particular the determination of the $\pi-\pi$-stacking distance impossible.

*Corresponding author. E-mail: s.rathgeber@uni-mainz.de.

 Published on Web 11/25/2009 

We revisited the somewhat forgotten procedure proposed by Milberg already in 1962, which allows the suppression of any (arbitrary) isotropic contribution to the scattering in order to separate the purely anisotropic scattering.[18−20] In this way we were able to separate scattering features originating from correlations along the fiber axis and from $\pi-\pi$-stacking for the investigated system which shows limited longer ranged order only.

The particular system under investigation are anthracene containing poly(arylene-ethynylene)-*alt*-poly(arylene-vinylene)s (PAE−PAVs) with general constitutional unit: (−Ph−C≡C−Anthr−C≡C−Ph−CH=CH−Ph−CH=CH−)$_n$ studied by means of wide-angle X-ray scattering (WAXS). This work has been carried out with the goal to establish a correlation between the structural ordering of donor polymers and their photovoltaic response in polymer−fullerene bulk heterojunctions for which a basic understanding of the bulk structural properties as well as of their response to thermal annealing is essential. The structural ordering is characterized in terms of positional correlations along the backbones, interlayer and $\pi-\pi$ stacking distances between different chains as well as by the degree of order in terms of number of lattice planes per domain. PAE−PAVs have proven their effectiveness as donor photovoltaic materials in both polymer−fullerene and polymer−vinazene solar cells.[13−17] Their semirigid nature moreover offers the possibility to readily tune the $\pi-\pi$-stacking ability and thus their photophysical properties by grafting of linear and/or branched side chains.

This paper is presented as follows: first, we give a short outline of the evaluation method for fiber scattering spectra proposed by Milberg. Second, we discuss the effect of annealing on the *as synthesized* polymers on the basis of results obtained for powder samples by means of dynamic scanning calorimetry and WAXS before we derive structural details as e.g. correlations along the backbone direction and $\pi-\pi$-stacking distances from the WAXS filament spectra. Last but not least, we correlate the so obtained $\pi-\pi$-stacking distances with the photophysical properties of the polymers. The photovoltaic response in polymer-heterojunctions is discussed elsewhere.[21]

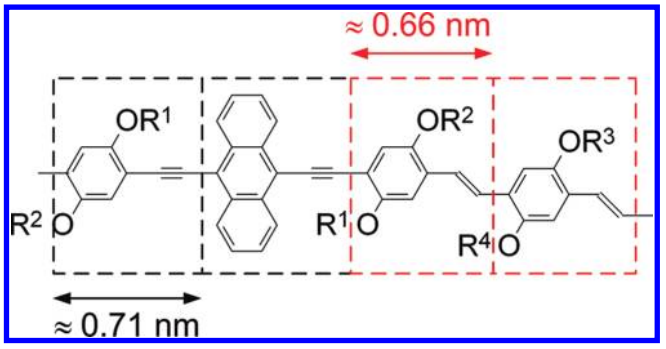


**Figure 1.** Sketch of the structure of the anthracene containing poly(*p*-phenylene−ethynylene)-*alt*-poly(*p*-phenylene−vinylene)s and approximate dimensions of the building blocks calculated under the assumption of a fully stretched conformation. A summary of the attached side chains is given in Table 1.

## Experimental Section

**Samples.** The synthesis of the anthracene containing poly(*p*-phenylene−ethynylene)-*alt*-poly(*p*-phenylene−vinylene)s, abbreviated **AnE-PV**, with general constitutional unit: (−Ph−C≡C−Anthr−C≡C−Ph−CH=CH−Ph−CH=CH−)$_n$ are products from the Horner−Wadsworth−Emmons polycondensation reaction of dialdehydes and bisphosphonate esters carried out on the basis of a known synthetic protocol. For details on the synthesis see refs 21 and 22. The general structure of the polymers is depicted in Figure 1; Table 1 defines the nomenclature. All polymers except for **AnE-PVaa** and **AnE-PVac** are soluble in common organic solvents such as chloroform, tetrahydrofuran (THF), dichloroethane, chlorobenzene and toluene. The chemical structures of the polymers were confirmed through nuclear magnetic resonance, infrared- and ultraviolet−visible spectroscopy as well as elemental analysis. Number- and weight-average molecular weights, $M_n$ and $M_w$, as well as the polydispersity PDI = $M_w/M_n$ obtained from gel permeation chromatography (GPC) (THF as eluent, polystyrene as standards) are summarized in Table 1. Thermogravimetric analysis reveals that the polymers are thermostable; 5% weight loss was recorded for all polymers above 300 °C. The polymer **AnE-PVstat** is a statistic copolymer comprising arylene-ethynylene units and arylene-vinylene units with $R^1 = R^2 =$ octyl and $R^1 = R^2 =$ 2-ethylhexyl substitution (ratio 1:1:1:1) in a statistic manner. It thus comprises a mixture of the repeating units of the polymers **AnE-PVaa**, **-ab**, **-ba**, and **-bb.**

**Thermal Analysis.** Differential scanning calorimetry (DSC) measurements were carried out on a Mettler DSC 30 with a cell purged with nitrogen. Calibration for temperature and enthalpy changes was performed using an Indium standard. The temperature was changed between 0 and 250 °C with a heating/cooling rate of 10 K/min. In total two heating−cooling cycles were performed on each sample. Transition temperatures were determined from the peak maxima of the first heating run and are listed in Table S1 (Supporting Information). Thermogravimetric analysis (TGA) was performed on a Mettler TA-300-thermal analyzer operating under air atmosphere. The samples were heated from 0 to 700 °C with a heating rate of 10 K/min. The decomposition temperatures determined at 5% weight loss, lie above 300 °C for all polymers. Exact values for the decomposition temperatures are listed in ref 21.

**Wide-Angle Scattering Experiments.** WAXS experiments in transmission geometry were carried at a wavelength

**Table 1. Properties of the Anthracene Containing Poly(*p*-phenylene−ethynylene)-*alt*-poly(*p*-phenylene−vinylene)s[a]**

| name **AnE-PV** | $R^1$ | $R^2$ | $R^3$ | $R^4$ | $M_n$ [g/mol] | $M_w$ [g/mol] | PDI | soluble | $T_{ex}$ [°C] |
|---|---|---|---|---|---|---|---|---|---|
| **-aa** | octyl | octyl | octyl | octyl | b | b | b | — | 120 |
| **-ad** | octyl | octyl | decyl | decyl | 19300 | 54000 | 2.79 | √ | 120 |
| **-ae** | octyl | octyl | dodecyl | dodecyl | 13300 | 26200 | 1.97 | √ | 120 |
| **-ab** | octyl | octyl | 2-EHl | 2-EH | 40000 | 141600 | 3.54 | √ | 120 |
| **-ac** | octyl | octyl | methyl | 2-EH | b | b | b | — | 120 |
| **-ba** | 2-EH | 2-EH | octyl | octyl | 25500 | 77800 | 3.05 | √ | 120 |
| **-bb** | 2-EH | 2-EH | 2-EH | 2-EH | 15800 | 47200 | 2.98 | √ | 120 |
| **-cc** | methyl | 2-EH | methyl | 2-EH | 47500 | 91900 | 1.91 | √ | 190 |
| **-stat** | octyl | octyl | octyl | octyl | 27500 | 56000 | 2.04 | √ | 120 |
| | octyl | octyl | 2-EH | 2-EH | | | | | |
| | 2-EH | 2-EH | octyl | octyl | | | | | |
| | 2-EH | 2-EH | 2-EH | 2-EH | | | | | |

[a] $R^i$ = side chains as defined in Figure 1($i$ = 1, 2, 3, 4; 2-EH = 2-ethylhexyl), $M_n$ = number-average molecular weight, $M_w$ = weight-average molecular weight, PDI = polydispersity, their solubility in common solvents (see also Experimental Section), and $T_{ex}$ = extrusion temperature for filament preparation. [b] Not determined.

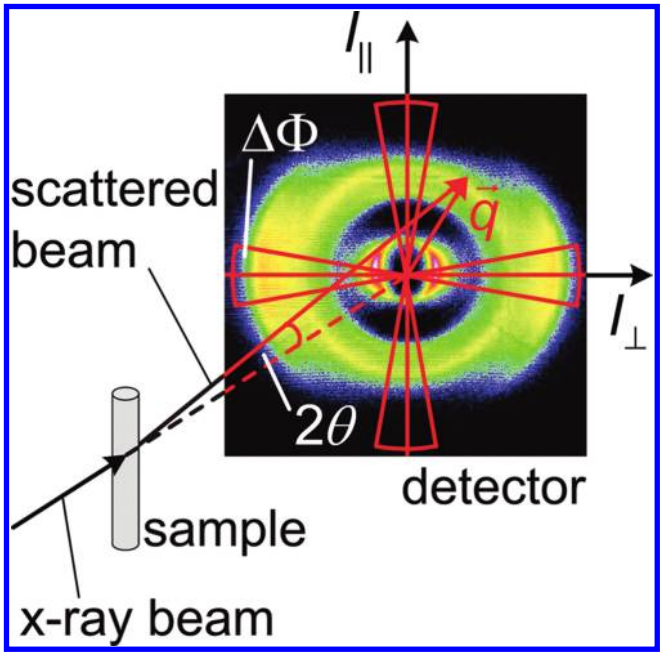


**Figure 2.** Sketch of the transmission WAXS setup and principle of the evaluation of the two-dimensional scattering pattern obtained for the filaments.

$\lambda = 0.154$ nm (Cu Kα radiation). A two pinhole collimation system provides a beam of about 0.5 mm in diameter. The diffraction pattern were recorded with a collection time of 1 h (powders) and 3 h (filaments) on a two-dimensional area detector (Bruker HI-STAR, 1024 × 1024 pixels). With the detector located at a sample-to-detector distance of 7.5 cm (determined by means of a silver behenate standard) a $q$ range between 2 $nm^{-1}$ and 23 $nm^{-1}$ were covered ($|\vec{q}| = q$ = norm of the scattering vector). The $q$ resolution of the WAXS experiment was estimated from the full-width-at-half-maximum (fwhm) of the silver behenate Bragg peaks to be $\Delta q_G = (0.43 \pm 0.02)$ $nm^{-1}$ under the assumption that the peak broadening in the silver behenate is solely due to limited instrumental resolution. For a sketch of the setup, see Figure 2.

Filaments with a diameter of about 0.7 mm were prepared by means of microextrusion at temperatures at which the polymers are plastically deformable (190 °C for **AnE-PVcc** and 120 °C for all other samples). Filaments and powder samples were measured in quartz capillaries (Hilgenberg GmbH) with a diameter of 1.5 mm. The two-dimensional data are corrected for background scattering from the quartz capillary. The detector pattern obtained for the powder and filament samples were subsequently radial averaged (over an azimuth angle of $\Phi = 0°$ to 360°) in order to obtain the radial averaged intensity $I$. For the determination of the scattering intensities in the direction perpendicular $I_{\perp}$ and parallel to the filament axis $I_{\parallel}$, the data obtained for the filaments were in addition averaged over an azimuth angle of $\Delta\Phi = \pm 10°$ around the horizontal (perpendicular to filament axis) and vertical direction (parallel to filament axis), respectively (see Figure 2). The averaged data are plotted as a function of the norm of the scattering vector $|\vec{q}| = q = 4\pi/\lambda \sin(\theta)$, where $2\theta$ is the scattering angle. From the positions $q^*$ of the Bragg peaks the distance of the corresponding crystal lattice planes $d = 2\pi/q^*$ can be derived. The peak intensity as well as the widths of the Bragg peaks can be taken as a measure of the degree of order. Because of the fact that the density of the powder samples might vary from sample to sample and with temperature, we consider the width of the Bragg peaks to be the more reliable quantity for determing the degree of order. The domain size $\xi$ can be understood as a length scale over which positional correlations are present and can be estimated by the Scherrer's formula $\xi = 2\pi/\Delta q^*$ where $\Delta q^*$ is the actual fwhm of the Bragg peak. The measured width $\Delta q_M$ is due to a convolution of the Gaussian shaped instrumental broadening function and the actual width of the Bragg peaks $\Delta q^*$ which can be approximated by a Lorentzian.[18] The instrumental peak broadening was estimated from a Gaussian fit to the silver behenate Bragg peaks to be $\Delta q_G = (0.43 \pm 0.02)$ $nm^{-1}$ (see above). On the basis of $\Delta q_M$ and $\Delta q_G$ the actual width of the Bragg peaks $\Delta q^*$ of the polymer samples was determined numerically. The number of lattice planes per domain $n = \xi/d = q^*/\Delta q^*$ is discussed as a measure of the degree of order.

**Photophysical Investigations.** Fluorescence measurements were performed with the CD900FS steady state photon counting fluorescence spectrometer (Edinburgh Analytical Instruments) with a high pressure xenon lamp as excitation source. The spectral slit widths of the excitation monochromator and emission monochromator were 0.9 and 3.6 nm, respectively. The polymer filaments were fixed onto an adjustable *xyz*-support and mounted into the spectrometer with the filament axis parallel to the monochromator slits. The samples exhibit a very large absorbance in the visible spectral region. In order to reduce pre- and postfilter effects the frontal geometry was chosen for excitation as well as for the measurement of the fluorescence. Because of the nonuniform cylindrical shape of the filaments a large amount of nonabsorbed excitation light as well as contributions originating from nonregularly traveling excitation light, appearing at other wavelengths superimpose the fluorescence. To minimize these contributions, the excitation and emission wavelength were spectrally separated at least by 10 nm. The measured fluorescence spectra were corrected with respect to the spectral characteristic of the spectrometer and are presented as photon spectra but are not corrected with respect to the flatness of the intensity distribution of the xenon lamp in the used spectral region (500−700 nm).

**Theory.** In order to obtain structural information on (weakly) oriented fiber samples Milberg proposed a simplified cylindrical distribution function which can be easily obtained from the two-dimensional detector pattern.[18−20] The radial distribution function $P(r)$ gives the number of interatomic vectors connecting two scattering units at distance $|\vec{r}| = r$. The cylindrical distribution function $P'(r,\alpha)$ of an uniaxially oriented sample gives the number of interatomic vectors connecting two scattering units which make an angle α with the axis of orientation in real space:

$$P(r) = \frac{1}{2}\int_0^{\pi} P'(r,\alpha)\,\sin\alpha\,\mathrm{d}\alpha \qquad (1)$$

The contribution to the total scattering intensity solely due to nonisotropic scattering is then given by the Fourier transform of the difference between of $P'(r,\alpha)$ and $P(r)$:

$$\int_0^{\infty} [P'(r,\alpha) - P(r)]\,\exp[-2\pi i\,\vec{q}\,\vec{r}\,]\,\mathrm{d}\vec{r}$$

$$= I(q,\Phi) - \frac{1}{2}I_0(q) = I'(q,\Phi) \qquad (2)$$

Here, [by use of eq 1]

$$I_0(q) = \int_0^{\pi} I(q,\Phi)\,\sin\Phi\,\mathrm{d}\Phi$$

is the radial averaged intensity of the anisotropic two-dimensional detector pattern. Thus, in the difference $I'(q,\Phi)$ all isotropic contribution, e.g., due to nonperfect orientation or amorphous parts of the samples, are automatically omitted.

## Results and Discussion

**DSC Measurements.** The *as prepared* samples (powders) show an endothermic transition at low temperatures

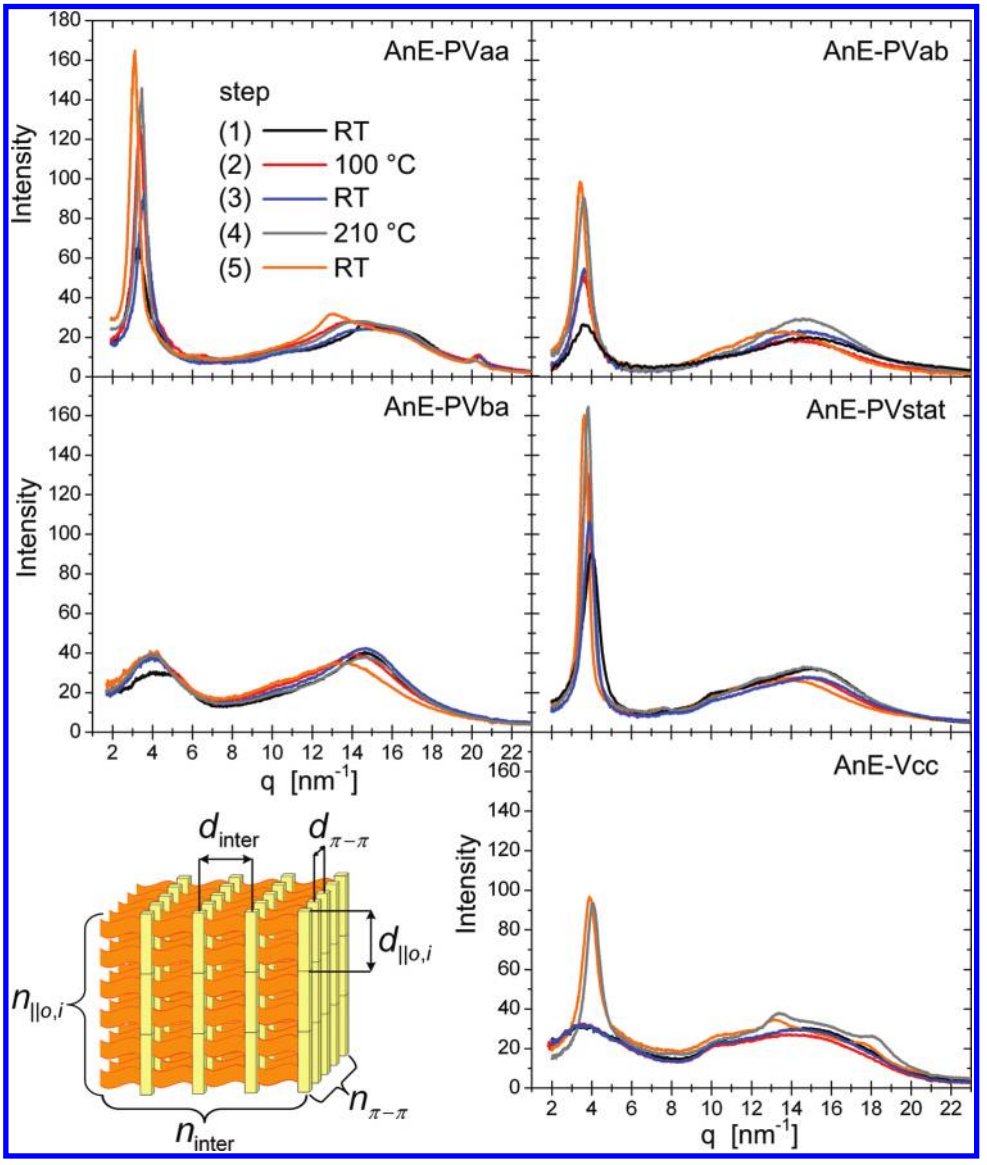


**Figure 3.** Representative WAXS results obtained for the powder samples after different annealing steps. A sketch of the layered structure of the nonamorphous **AnE-PV** polymers is also included.

(45 °C-75 °C) and a broad exothermic transition at temperatures between 170 and 250 °C in the first heating run only. No transitions are visible in the subsequent heating and cooling cycles. The DSC thermograms obtained during the first heating run and a summary of the transition temperatures are included in the Supporting Information, Figure S1 and Table S1, respectively. In combination with the information obtained from the scattering experiments these transitions are presumed to originate from an order−disorder transition (melting) of the side chains (low temperature transition) and from a backbone-reorganization and high temperatures. Because of the fact that these transitions are not visible in the subsequent DSC cooling and heating runs they must result from nonequilibrium structures frozen in as a result of the preparation process. The absence of the low-temperature transition in the subsequent DSC runs indicates that the side chains are most likely not crystalline in the equilibrium structure. The transition at high temperatures leads to an improved interlayer stacking which is preserved during cooling the sample back to room temperature and therefore can be assumed to be the equilibrium structure (see also scattering results). The backbone reorganization transition is not visible for the samples which are according to the scattering results amorphous.

**Bulk Properties: Effect of Annealing.** We investigated the effect of annealing on the structural properties of the copolymers **AnE-PV**. WAXS experiments were performed on the *as synthesized* powders at room temperature, (1), at 100 °C that is above the side chain melting temperature, (2), and at 210 °C where the anthracene containing copolymers are known to undergo backbone reorganization, (4). In order to study the effect of annealing on the structural properties at room temperature, the samples were cooled down back to room temperature and measured again after each annealing step (3 + 5). Figure 3 shows the WAXS spectra taken at different steps of the annealing procedure for some representative samples: **AnE-PVaa**, **-ab**, **-ba**, and **-cc** and **-stat**. A summary of the scattering spectra of all samples is given in the Supporting Information (see Figure S2).

The WAXS experiments (combination of powder and filament experiments) reveal that the polymers **AnE-PVaa**, **-ad**, **-ae**, **-ac**, and **-ab** bearing linear octyl side chains at $R^1$ and $R^2$ on the more rigid part of the conjugated backbone, i.e. the arylene-ethynylene segment, as well as the statistic

copolymer **AnE-PVstat** arrange in a stacked structure. This layered structure comprises $\pi-\pi$-stacks of the backbones ($\pi-\pi$-stacking distance $d_{\pi-\pi}$) which are separated by interlayers (distance $d_{inter}$) built by the side chains. For a sketch of the structure see Figure 3. The first sharp Bragg peak originates from interlayer stacking (see Figure 3 and Figure S2). The distances of the crystal lattice planes $d_{inter} = 2\pi/q^*_{inter}$ can be obtained from the positions $q^*_{inter}$ of the Bragg-peaks. Table 2 summarizes the interlayer distances $d_{inter}$. The peak intensity as well as the widths of the Bragg-peaks can be taken as a measure of the degree of order. From the actual widths of the Bragg peaks $\Delta q^*_{inter}$ (corrected for instrumental broadening, see Experimental Section) the interlayer correlations length $\xi_{inter} = 2\pi/\Delta q^*_{inter}$ as well as the number of interlayer lattice planes per domain $n_{inter} = \xi_{inter}/d_{inter}$ (see Table 2) as a measure of the degree of order can be calculated. The peak positions $q^*_{inter}$, the peak widths $\Delta q^*_{inter}$ and the correlation lengths $\xi_{inter}$ are listed in Table S2 (Supporting Information). Correlations along the backbone direction, contributions from the (amorphous) side chains as well as from $\pi-\pi$-stacking all appear as broad peaks in the same $q$ region (10 $nm^{-1}$– 18 $nm^{-1}$) and, thus, cannot be separated for the powder samples. They will be discussed in the context of the results obtained from filament samples (see below).

The degree of order, measured in terms of $n_{inter}$, increases when the samples are annealed at temperatures above the side chain melting temperature and backbone reorganization temperature, respectively. An enhanced order can be preserved after both annealing steps if the sample is cooled back to room temperature. For the polymers with all linear substitution (**AnE-PVaa**, **-ad**, **-ae**) annealing results in an increase in the degree of order by about 60% to 90% after the first and an additional 100% to 140% after the second annealing step. Interestingly, the polymer with the shortest (octyl) and longest (dodecyl) side chains attached to the vinylene unit [**AnE-PVaa** ($n_{inter} \approx 18$) and **-ae** ($n_{inter} \approx 12$)] show a higher degree of order after both annealing steps than **AnE-PVad** ($n_{inter} \approx 7$) carrying decyl side chains. At $T = 210$ °C a particularly long ranged order is found for the polymer **AnE-PVae** ($n_{inter} \approx 24$) which cannot be preserved when cooling back to room temperature. The partly asymmetric substituted polymer **AnE-PVac** show a comparable behavior. After the first annealing step the degree of order increases by almost 200% to $n_{inter} \approx 9$ but heating to the backbone recrystallization temperature leads to no further improvement: the improved order at 210 °C ($n_{inter} \approx 15$) cannot be preserved when cooling back to room temperature ($n_{inter} \approx 10$). Obviously, in the polymers **AnE-PVae** and **-ac** with the longest linear side chains or an asymmetric substitution at the vinylene unit, respectively, the optimal arrangement of the backbone is disturbed below the side chain melting temperature when the side chains, that are more flexible at temperatures above the side chain melting temperature, strive for optimal packing.

The samples **AnE-PVab** and **AnE-PVstat** containing bulky 2-ethylhexyl side chains exhibit a smaller improvement of the order at room temperature in response to annealing (about 50% to 60% after the first and another 70% to 80% after the second step). However, remarkably is the degree of order ($n_{inter} \approx 15$) of the statistic copolymer **AnE-PVstat** after both annealing steps which compares very well to that of **AnE-PVaa** with all octyl substitution having the highest degree of order. This is even more notable if one considers that the statistic copolymer contains a mixture of the repeating units of the polymers **AnE-PVaa**, **-ba**, **-ab**, and **-bb** and that the polymers **AnE-PVba** and **AnE-PVbb** with

**Table 2. WAXS Results Obtained for the Powder Samples at Different Steps of the Annealing Procedure**[a]

| T [°C] | | AnE-PVaa | -ad | -ae | -ab | -ac | -cc | -stat | -ba | | -bb | |
|---|---|---|---|---|---|---|---|---|---|---|---|---|
| | | | | | | | | | 1st | 2nd | 1st | 2nd |
| RT | $d_{inter}$ | 1.92±0.01 | 1.93±0.01 | 1.95±0.01 | 1.69±0.01 | 1.56±0.01 | 1.71±0.01 | 1.58±0.01 | 1.60±0.02 | 1.19±0.02 | 1.35±0.01 | 1.39±0.01 |
| | $n_{inter}$ | 3.9±0.2 | 1.9±0.1 | 3.3±0.3 | 2.2±0.1 | 3.2±0.2 | 1.3±0.1 | 5.4±0.3 | 1.1±0.1 | 4.4±0.4 | 1.3±0.1 | 21±3 |
| 100 | $d_{inter}$ | 1.87±0.01 | 1.94±0.01 | 2.02±0.01 | 1.76±0.01 | 1.66±0.01 | 1.73±0.01 | 1.67±0.01 | 1.59±0.02 | 1.14±0.02 | 1.48±0.01 | 1.52±0.01 |
| | $n_{inter}$ | 10.3±0.8 | 3.6±0.2 | 6.0±0.4 | 3.4±0.2 | 9.9±0.9 | 1.2±0.1 | 7.9±0.5 | 1.2±0.1 | 6±1 | 1.5±0.1 | 33±6 |
| RT | $d_{inter}$ | 1.77±0.01 | 1.87±0.01 | 1.95±0.01 | 1.72±0.01 | 1.53±0.01 | 1.73±0.01 | 1.62±0.01 | 1.56±0.01 | | 1.33±0.01 | 1.39±0.01 |
| | $n_{inter}$ | 7.4±0.5 | 3.4±0.2 | 5.4±0.3 | 3.5±0.2 | 9.4±0.8 | 1.3±0.1 | 8.1±0.5 | 1.0±0.1 | | 1.1±0.1 | 19±2 |
| 210 | $d_{inter}$ | 2.03±0.01 | 2.09±0.01 | 2.15±0.02 | 1.82±0.01 | 1.85±0.01 | 1.60±0.01 | 1.73±0.01 | 1.63±0.01 | | 1.39±0.01 | |
| | $n_{inter}$ | 14±2 | 6.7±0.4 | 24±4 | 7.6±0.5 | 15±2 | 5.8±0.3 | 15±2 | 1.4±0.1 | | 1.0±0.1 | |
| RT | $d_{inter}$ | 1.83±0.01 | 1.88±0.01 | 1.93±0.01 | 1.75±0.01 | 1.65±0.01 | 1.54±0.01 | 1.65±0.01 | 1.60±0.01 | | 1.39±0.01 | |
| | $n_{inter}$ | 18±2 | 7.0±0.4 | 12±1 | 6.0±0.3 | 10.3±0.7 | 6.3±0.4 | 15±1 | 1.2±0.1 | | 1.0±0.1 | |

[a] $d_{inter}$ = interlayer distance and corresponding number of lattice planes $n_{inter}$ per domain. RT denotes room temperature. Distances are given in nanometers.

2-ethylhexyl side chains attached to the arylene-ethynylene units are amorphous (see below).

The polymers **AnE-PVba** and **AnE-PVbb** with bulky, branched 2-ethylhexyl attached to the arylene-ethynylene moiety exhibit only two broad peaks corresponding to the nearest neighbor correlations of the backbones and side chains, respectively. They show basically no long-range order ($n_{inter} \approx 1$). The small sharp peak on top of the first broad Bragg peak observed for the sample **AnE-PVbb** reveals some crystalline fraction (see Figure S2 in the Supporting Information) in the *as synthesized* sample which however (almost) disappears if the sample is annealed at 210 °C. The *as synthesized* polymer **AnE-PVba** also shows a second peak corresponding to a somewhat longer-ranged structure. This peak cannot be resolved anymore as soon as the sample is annealed at 100 °C.

The asymmetric substituted sample **AnE-PVcc**, i.e., $R^1 = R^3$ = 2-ethylhexyl and $R^2 = R^4$ = methyl, shows a distinct behavior. It is amorphous at temperatures up to about 100 °C. However, when the sample is annealed up to the backbone recrystallization temperature it reorganizes into a stacked structure comparable to that of the polymers bearing linear octyl side chains at $R^1$ and $R^2$ (**AnE-PVa**$_*$). The degree of order ($n_{inter} \approx 6$) can be preserved when the sample is cooled back to room temperature.

The absolute values for the interlayer stacking distances determined after both annealing steps - which we consider to correspond to the equilibrium structure - can be compared to the calculated length of the fully extended side chains $l_{SC}$ plus the heigth of the phenyl ring ($l_{Ph} \approx 0.24$ nm). For details on the calculation see Scheme S1 in the Supporting Information. The interlayer distance is always smaller than $2l_{SC} + l_{Ph}$. If the side chains were in a fully extended conformation, this would require a structure where the side chains from neighboring back bones would either have to strongly interdigitate or to exhibit a significant tilt relative to the backbone. Since the endothermic peak of the side chain melting is missing in the higher DSC runs there should not be significant side chain crystallization leading to structures where the stacked side chains arrange in well-defined digitated or tilted structures. Most likely they digitate in a loose manner. This would be in accordance with the observation of phenyl ring correlations between the stacked backbones and some preferred orientation of the side chains perpendicular to the backbones (see discussion of the filament scattering results). As expected as longer the linear side chains attached to the vinylene unit as larger the interlayer stacking. However, the increase in $d_{inter}$ is small (5%). Shorter (even though more bulky) 2-ethylhexyl side chains or even asymmetric substitution involving a small methyl group lead to a reduction of the interlayer spacing. Only for the fully asymmetric substituted polymer **AnE-PVcc** the interlayer distance suggests an extended conformation of the side chains, provided that the stacking takes place in such a way that 2-ethylhexyl and methyl group stack on top of each other and build the interlayer

**Filaments: Determination of $\pi-\pi$ Stacking Distances.** The limited structural order in polymer crystals leads to significant line broadening and the absence (fast decay) of higher order scattering features. In addition scattering contributions from the amorphous side chains, from correlations along the backbone direction as well as from $\pi-\pi$-stacking all contribute to the overall scattering intensity in a comparable q region. Therefore, distinction of the different scattering contributions is often difficult or impossible from isotropic samples. Microextrusion does not induce crystallization, it rather leads to an alignment of the microdomains in such a way that the backbones are oriented along the fiber axis. Thus, the amorphous samples **AnE-PVbb** and **-ba** do not show any alignment after extrusion. The two-dimensional detector pattern are isotropic (see Figure S3). Only first order correlation peaks corresponding to the mean interbackbone spacing and the mean side chain distance, respectively, are visible. A two-dimensional detector pattern (**AnE-PVab**) which is representative for those obtained for the extruded filaments of the nonamorphous samples is shown in the left part of Figure 4. The corresponding q-cuts are also included: the radial averaged intensity $I$ as well as $I_\perp$ and $I_\parallel$ obtained for the direction perpendicular and parallel to the filament axis, respectively. To Figure 4 analogous presentations for all samples are summarized in Figure S3 (Supporting Information). The sharp Bragg peaks at low q values in horizontal direction are due to interlayer stacking. At larger $q$ values, peaks corresponding to $\pi-\pi$-stacking should appear in the same direction whereas Bragg peaks resulting from correlations along the polymeric backbone should appear in the vertical direction. No clear Bragg-peaks can be resolved in the high q region even though the scattering is clearly asymmetric as can be seen from respective $q$ cuts (see Figure 4 and Figure S3). The limited degree of structural order of the samples, but in particular the isotropic scattering contributions from the amorphous side chains appearing in

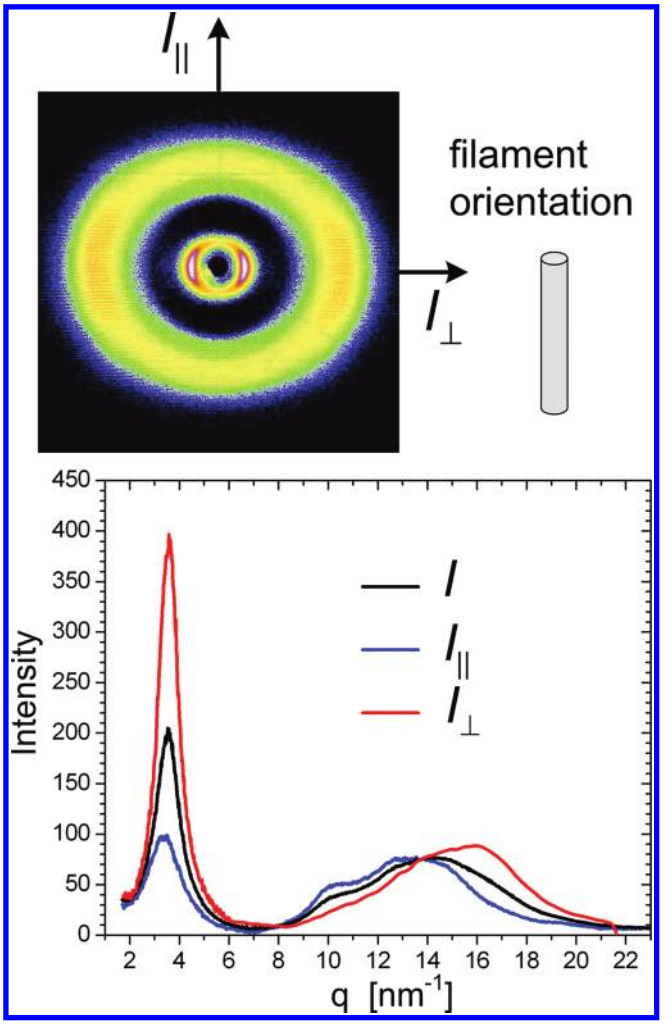


**Figure 4.** Representative WAXS results (**AnE-PVab**) obtained for the filament samples. Left: two-dimensional detector pattern. Right: corresponding $q$ cuts, $I_\parallel$ (blue) and $I_\perp$ (red), as well as the radial averaged intensity $I$ (black).

the same $q$ region as well as not perfect alignment of the microdomains after microextrusion makes a direct evaluation of the unisotropic scattering spectra impossible.

However, one can discriminate isotopic contributions by subtraction of the radial averaged ($\Phi = 0$ to $2\pi$) intensity $I$ from $I_{\parallel}$ and $I_{\perp}$. In order to obtain sufficient statistics the latter were averaged over an azimuth angle $\Delta\Phi = \pm 10°$ around the vertical ($\parallel$ to filament axis) and horizontal ($\perp$ to filament axis) detector direction, respectively (see Figure 2). In this way the purely anisotropic scattering contributions parallel $I_{\parallel o}$ and perpendicular $I_{\perp o}$ to the filament axis are obtained (see also Theory Section). Figure 5 presents the results for all nonamorphous samples. Table 3 and 4 summarize the lattice plane distances as well as the number of planes per domain determined from the peak positions and widths observed in $I_{\parallel o}$ and $I_{\perp o}$. The peak positions, the peak widths and the resulting correlation lengths are presented in Table S3 (Supporting Information).

The q cuts perpendicular to the filament axes $I_{\perp o}$ show peaks originating from interlayer and $\pi-\pi$-stacking. The interlayer stacking has been already discussed on the basis of the results obtained for the powder samples. The interlayer stacking distances $d_{\text{inter}}$ of the filaments are summarized in Table 3. Despite for the polymers **AnE-PVaa** and **ac** there is within the error bars quantitative agreement between the interlayer distances obtained for the filaments and corresponding annealed powder samples, respectively. Note that extrusion has been performed at 190 °C for **AnE-PVcc** and 120 °C for all other samples in order to allow for plastic deformation. Deviations observed for the two samples, **AnE-PVad** and **-ac**, are most likely due to the fact that the annealing of the powder samples was performed at a lower temperature (100 °C) than that used for extrusion. The interlayer distances determined for the filaments are approximately 6% (**AnE-PVad**) and 5% (**AnE-PVac**) larger than the values determined for the corresponding annealed powder samples.

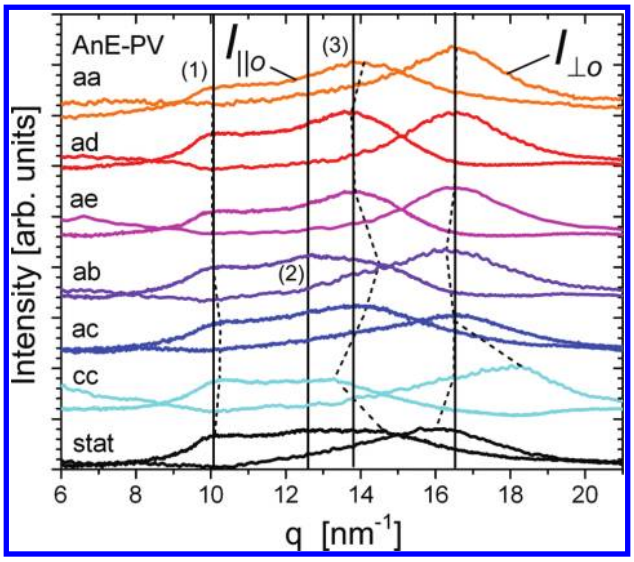


**Figure 5.** Scattering intensities perpendicular and parallel to the filament axis after subtraction of the isotropic contribution. The lines denote the peak positions listed in Table S3. For better visibility the curves are shifted along the y-axis.

The $\pi-\pi$-stacking distances $d_{\pi-\pi}$ are presented in Figure 6. Table 4 summarizes the $d_{\pi-\pi}$ values as well as the corresponding number of lattice planes per domain $n_{\pi-\pi}$. The $\pi-\pi$-stacking distances are found to be the same $d_{\pi-\pi} = (0.380 \pm 0.002)$ nm for the polymers carrying all-linear side chains (**AnE-PVaa**, **-ad**, **-ae**) as well as the partly asymmetric substituted polymer **AnE-PVac**. The polymers **AnE-PVab** and the polymer **AnE-PVstat** containing bulky, branched 2-ethylhexyl side chains have larger $\pi-\pi$-stacking distances, $d_{\pi-\pi} = 0.386$ and 0.393 nm, respectively. $\pi-\pi$-stacking domains comprise 5 to 7 $\pi-\pi$-stacking layers for the polymer with all-linear side chains (**AnE-PVaa**, **-ad**, **-ae**) and about 3 to 4 layers for the polymer containing bulky, branched 2-ethylhexyl side chains (**AnE-PVab** and **-stat**). Thus, even though the polymer **AnE-PVstat** shows comparable degree of order as the polymer **AnE-PVaa** in respect to interlayer stacking the degree of order in respect to $\pi-\pi$-stacking is reduced and the $\pi-\pi$-stacking distance increased.

The asymmetric substituted polymer **AnE-PVcc** shows a distinct behavior. Note that extrusion was performed at 190 °C. Two peaks originating most likely from two polymorphs are observed: one with $d_{\pi-\pi} = 0.379$ nm which corresponds well to the value found for the polymers carrying linear side chains whereas the second has a significantly lower $\pi-\pi$-stacking distance $d_{\pi-\pi} = 0.344$ nm. The lower $\pi-\pi$-stacking distance goes hand in hand with a higher degree of order. Positional correlations are lost over 8 ($d_{\pi-\pi} = 0.344$ nm) and 3 ($d_{\pi-\pi} = 0.379$) lattice planes, respectively. The latter

**Table 4. Emission Data of the AnE-PV Polymers Ordered with Respect to Decreasing Emission Maximum together with the $\pi-\pi$-Stacking Distances $d_{\pi-\pi}$ and Corresponding Numbers of Lattice Planes $n_{\pi-\pi}$ per Domain[a]**

| polymer **AnE-PV** | $\lambda_{f(0\rightarrow0)}$ | $\lambda_{f(0\rightarrow1)}$ | $d_{\pi-\pi}$ | $n_{\pi-\pi}$ |
|---|---|---|---|---|
| **-cc** | | 695 | 0.379 ± 0.004 | 3.2 ± 0.5 |
| | | | 0.344 ± 0.002 | 8.4 ± 0.8 |
| **-aa** | 620 | 685 | 0.380 ± 0.002 | 6.5 ± 0.5 |
| **-ad** | 625 | 685 | 0.380 ± 0.002 | 4.7 ± 0.3 |
| **-ac** | 620 | 685 | 0.381 ± 0.002 | 3.2 ± 0.3 |
| **-ae** | 620 | 680 | 0.380 ± 0.002 | 4.7 ± 0.2 |
| **-ab** | 620 | 680 | 0.386 ± 0.002 | 4.2 ± 0.2 |
| **-stat** | 620 | 675 | 0.393 ± 0.003 | 3.7 ± 0.4 |
| **-ba** | | 650 | | |
| **-bb** | 605 | 650 | | |

[a] Underlined are the main emission peaks. Wavelength and distances are given in nanometers.

**Table 3. WAXS Results Obtained for the Filaments from $I_{\perp o}$ and $I_{\parallel o}$[a]**

| $q$ cut | | **AnE-PVaa** | **-ad** | **-ae** | **-ab** | **-ac** | **-cc** | **-stat** |
|---|---|---|---|---|---|---|---|---|
| $I_{\parallel o}$ | $d_{\parallel o,1}$ | 0.61 ± 0.01 | 0.63 ± 0.01 | 0.63 ± 0.01 | 0.62 ± 0.01 | 0.61 ± 0.01 | 0.61 ± 0.01 | 0.62 ± 0.01 |
| | $n_{\parallel o,1}$ | 3.7 ± 0.3 | 2.7 ± 0.2 | 2.3 ± 0.1 | 4.5 ± 0.5 | 3.9 ± 0.4 | 4.4 ± 0.4 | 5.5 ± 0.7 |
| | $d_{\parallel o,2}$ | | | | 0.50 ± 0.01 | | | 0.51 ± 0.02 |
| | $n_{\parallel o,2}$ | | | | 3.3 ± 0.3 | | | 3.2 ± 0.4 |
| | $d_{\parallel o,3}$ | 0.45 ± 0.01 | 0.45 ± 0.01 | 0.45 ± 0.01 | 0.43 ± 0.01 | 0.45 ± 0.01 | 0.47 ± 0.01 | 0.43 ± 0.01 |
| | $n_{\parallel o,3}$ | 2.7 ± 0.2 | 2.7 ± 0.2 | 2.9 ± 0.2 | 6.2 ± 0.8 | 2.2 ± 0.2 | 2.7 ± 0.2 | 2.7 ± 0.2 |
| $I_{\perp o}$ | $d_{\text{inter}}$ | 1.77 ± 0.01 | 1.99 ± 0.01 | 1.95 ± 0.01 | 1.76 ± 0.01 | 1.60 ± 0.01 | 1.53 ± 0.01 | 1.61 ± 0.01 |
| | $n_{\text{inter}}$ | 4.8 ± 0.3 | 3.1 ± 0.2 | 4.3 ± 0.2 | 4.7 ± 0.2 | 5.2 ± 0.4 | 5.4 ± 0.3 | 8.2 ± 0.5 |

[a] $d_{\text{inter}}$ = interlayer distance and $d_{\parallel o,i}$ = stacking distances along fiber axis ($i$ = 1, 2, 3) as well as the corresponding number of lattice planes per domain, $n_{\text{inter}}$ and $n_{\parallel o,i}$. Alignment temperature was 190 °C for **AnE-PVcc** and 120 °C for all other samples.

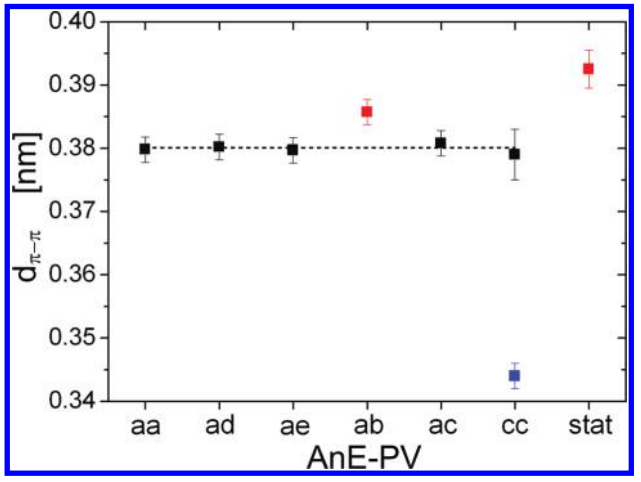


**Figure 6.** $\pi-\pi$ stacking distances obtained for the nonamorphous **AnE-PV** samples. Values are listed in Table 4.

value corresponds well to the value found for the polymers carrying linear side chains at the arylene-ethynylene segment.

From $I_{\parallel o}$ correlations in the direction of the fiber axis (backbone direction) can be determined. At maximum three scattering contributions can be approximately distinguished. The first peak [denoted (1) in Figure 5] corresponds to a length scale of $d_{\parallel o,1} \approx 0.62$ nm which agrees well with the dimensions of the phenylene−vinylene (PV) and phenylene−ethynylene (PE) building units. Assuming a fully extended conformation, the size of the PE and PV unit can be estimated to be 0.71 and 0.66 nm, respectively (see Figure 1). For details on the length estimation see Scheme S1 in the Supporting Information. However, experimentally smaller dimensions are found (e.g., for poly(phenyl vinylene) 0.605 nm).[23] Thus, most likely there is to some extent a preferred stacking of the phenyl rings along the backbone direction. Interestingly, if one compares the number of lattice planes, $n_{\parallel o,1}$ and $n_{\pi-\pi}$, better ordering in respect to $\pi-\pi$-stacking does not necessarily lead to stronger correlations along the polymer backbone. Polymers with bulky 2-ethylhexyl side chains attached to the vinylene unit (**AnE-PVab, stat**) as well as asymmetric substituted polymers (**AnE-PVac**, **-stat**) exhibit stronger correlations ($n_{\parallel o,1} \approx 4-6$) than polymers carrying linear side chains only ($n_{\parallel o,1} \approx 2-3$). Obviously, heterogeneous substitution imposes a more correlated arrangement of the backbones (relatively to each other) than attachment of side chains which are similar in nature (all linear). Two further peaks corresponding to length scales smaller than the backbone building unit can be resolved, corresponding to lattice spacings (2) $d_{\parallel o,2} \approx 0.50$ nm and (3) $d_{\parallel o,3}$ with values of approximately 0.43 nm for the polymers containing bulky 2-ethylhexyl side chains, 0.45 nm for the polymers with linear side chains at the arylene-ethynylene segment, up to 0.47 nm for the asymmetric substituted polymer. These values for $d_{\parallel o,3}$ correspond well to the side chain stacking distance found for alkyl substituted semiflexible polymers.[24] The fact that the side chains most likely contribute to the scattering $I_{\parallel o}$ indicates that there is some preferred orientation of the side chains perpendicular to the direction of the main chain. The second peak ($d_{\parallel o,2} \approx 0.50$ nm) cannot be assigned yet. However, it can only be clearly resolved for the polymers containing branched 2-ethylhexyl side chains (**AnE-PVab**, **-stat**) not including the asymmetric substituted polymers (**AnE-PVac**, **-cc**).

**Photophysics.** The polymer filaments exhibit a well measurable fluorescence with characteristic spectra in the

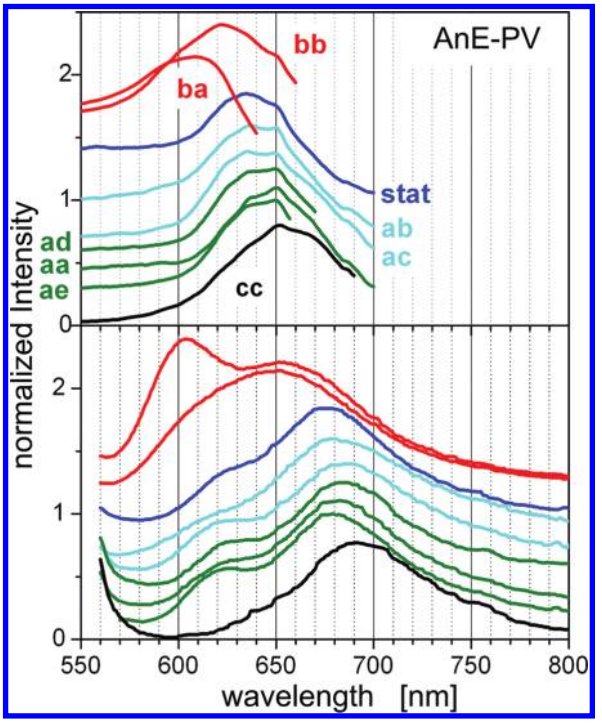


**Figure 7.** Excitation (top) and emission spectra (bottom) of the extruded fibers. Intensities are normalized to the peak intensities. For better visibility the spectra are shifted along the y-axis.

region from 560 to 800 nm. The shape of the spectra is essentially independent from the excitation wavelength after excitation in the region from 450 to 600 nm. With excitation above 600 nm in the region of the fluorescence band only the longer wavelength part of the fluorescence band is visible. Because of the unknown absorbed intensity and the strong scattering effects no conclusions on the fluorescence efficiency of the different polymers can be drawn. Fluorescence excitation spectra were measured in the region from 500 nm up to approximately 700 nm with emission wavelengths around 700 nm. They show a nearly flat intensity curve from 500 to 600 nm, but a pronounced increased intensity at longer wavelengths. This and the strong overlap of the excitation and emission spectra (see Figure 7) lead to the conclusion that at least two different emitting species on or near the surface of the polymer filaments exist, in which the more red absorbing one exhibits a higher fluorescence efficiency. However, measurements of the emission and excitation spectra from microtome- (mt-) sliced plane sections of filaments showed, that the cylindrical shape of the filaments does not significantly degrade the results obtained under our experimental conditions and that the results are also representative for the interior of the filaments.[9]

A general red shift of the emission spectra going from the solutions over the thin films to the extruded fibers is observed. The solution and thin film results are presented in ref 21. This is attributed to enhanced planarization of the conjugated backbones and organization in the bulk materials. The emission spectra of the nonamorphous sample (**AnE-PVaa**, **-ab**, **-ac**, **-ad**, **-ae**, and **-stat**) (see Figure 7) consist in general of two broad, vibronic features with the main peak located between 575 and 585 nm and a blue-shifted shoulder located between 520 and 525 nm. The emission peaks determined by a Gaussian fit are provided in Table 4 (rounded in 5 nm steps taking into account the broadness of the peaks) together with the $\pi-\pi$-stacking distance, $d_{\pi-\pi}$ and the number of lattice

planes per domain $n_{\pi-\pi}$. The data are ordered in respect to decreasing main emission band.

The energy difference of approximately 1300 $cm^{-1}$ between the two bands is similar to that found between the $0 \rightarrow 0$ and $0 \rightarrow 1$ transitions in the solution and thin film emission spectra.[21,25] Thus, we can readily assign the shorter wavelength band to the $S_{10} \rightarrow S_{00}$ radiative decay, originating from isolated backbone fluorophores, and the longer wavelength band as a superposition of the $S_{10} \rightarrow S_{01}$ transition and excimer-like emission resulting from enhanced planarization and closer organization of the backbones in the bulk materials. This interpretation is consistent with the observation that the emission spectrum of the polymer **AnE-PVcc** with the smallest $\pi-\pi$ stacking distance only shows one peak at 695 nm. No emission from isolated backbone fluorophores is observed. The emission spectra of the amorphous samples **AnE-PVba** and **-bb** ($S_{10} \rightarrow S_{00}$, 605 nm; $S_{10} \rightarrow S_{01}$, 650 nm) are significantly blue-shifted compared to those obtained for the nonamorphous samples. In the sample **AnE-PVbb** the $S_{10} \rightarrow S_{00}$ radiative decay originating from isolated backbone fluorophores represents the main emission peak. Thus, the differences in $\pi-\pi$-stacking are well correlated with the emission properties of the polymers. With the exception of the polymer **AnE-PVae** (with the longest linear side chain attached to the vinylene unit) one obtains that as higher the $d_{\pi-\pi}$ value the more blue-shifted is the main emission band. No correlation is found in respect to the degree of order of the $\pi-\pi$-stacking in terms of number of $\pi-\pi$ lattice planes per domain.

## Conclusions

We studied anthracene containing poly(*p*-phenylene−ethynylene)-*alt*-poly(*p*-phenylene−vinylene) polymers with general constitutional unit: $(-Ph-C\equiv C-Anthr-C\equiv C-Ph-CH=CH-Ph-CH=CH-)_n$ for applications as donor materials in organic photovoltaics by means of wide-angle X-ray scattering as well as by fluorescence spectroscopy. In order to tune the interchain interaction ($\pi-\pi$-stacking distance) and thus their structural and photophysical properties linear, branched as well as mixed linear and branched alkoxy side chains, respectively, have been attached to the backbone. The motivation of this study has been to characterize the structural properties of these materials and to establish a correlation to the emission properties of the polymers. Structural properties include the $\pi-\pi$- and interlayer stacking, correlations along the backbone as well as the degree of order of the stacking.

Special emphasis has been taken on an evaluation of fiber spectra that allows the deduction of structural details of polymer materials which most often show limited degree of order and thus are difficult to evaluate due to line broadening and absence of higher order scattering features. In addition isotropic scattering contributions due to not perfect alignment and from the amorphous side chains often blur the results and make in particular the reliable determination of the $\pi-\pi$-stacking distance impossible. We revisited the somewhat forgotten procedure proposed by Milberg already in 1962 which allows the suppression of any (arbitrary) isotropic contribution to the scattering from fiber spectra. In this way, the purely anisotropic scattering contribution can be separated.[18−20] By this method, which we would like to establish in the area of organic photovoltaics, we were able to separate scattering features originating from correlations along the fiber axis as, e.g., phenyl−ring correlation between different chains along the backbone direction and from $\pi-\pi$-stacking, respectively. Furthermore, it allows the quantification of the degree of order in respect to the number of lattice planes per domain.

The polymers with all-linear side chains attached close to the anthracenylene−ethynylene unit (AnE) show a layered structure comprising $\pi-\pi$-stacks of the backbones which are separated by interlayers built by the side chains. In contrast, attachment of branched side chains at the AnE unit leads to amorphous polymers. These structural differences are reflected in their photophysical properties. The emission spectra show broad emission peaks: one characteristic for isolated backbone fluorophores and a second peak resulting from a superposition of the $S_{10} \rightarrow S_{01}$ transition and excimer-like emission. The latter peak results from enhanced planarization of the backbones due to self-organization. In the amorphous polymers the contribution of isolated backbone fluorophores becomes dominant whereas it is suppressed in case that the $\pi-\pi$-stacking distance becomes small. The higher the $d_{\pi-\pi}$ value the more blue-shifted is the main emission band. However, no clear correlation of the emission peak position is found with respect to the degree of order of the $\pi-\pi$ stacking in terms of number of $\pi-\pi$ lattice planes per domain.

We also studied the effect of annealing and observed structural transitions which can be attributed to melting of the amorphous side chains and backbone reorganization, respectively. Both transitions lead to enhanced order in terms of interlayer stacking. For most polymers the increased order is preserved during cooling back to room temperature, but in some cases a decrease in structural ordering is observed. The decrease of structural ordering is believed to result from a distortion of the polymer backbone resulting from the strive of the side chains to find an optimum arrangement. Once annealed, the polymers do not show significant structural changes upon further heating. Structures that are stable over a wide temperature range should also lead to a more stable performance of polymer-based photovoltaic devices and, thus, should be beneficial for commercial applications.

**Acknowledgment.** S.R., D.A.M.E., and H.H. appreciate the financial support by the Deutsche Forschungsgemeinschaft (DFG) in the framework of the priority program SPP 1355 "Elementary processes in organic photovolatics".

**Supporting Information Available:** DSC thermograms obtained during the first heating run and a summary of the transition temperatures given in Figure S1 and Table S1, Figure S2 summarizing the temperature dependent radial averaged spectra obtained for the powder samples, Figure S3 containing the two-dimensional detector pattern as well as the one-dimensional spectra ($I$, $I_{\perp}$, $I_{\parallel}$) obtained for the filament samples, Table S2 and Table S3 containing the peak positions, the peak widths, and the resulting correlations lengths corresponding to the lattice spacings given in Table 2 as well as Table 3 and 4, respectively and a short explanation how the length of the side chains and backbone units were estimated (Scheme S1). This material is available free of charge via the Internet at http://pubs.acs.org.

## References and Notes

(1) Kroon, R.; Lenes, M.; Hummelen, J. C.; Blom, P. W. M.; de Boer, B. *Polym. Rev.* **2008**, *48*, 531.
(2) Hoppe, H.; Sariciftci, N. S. *J. Mater. Res.* **2004**, *19*, 1924.
(3) (a) Hoppe, H.; Saricifti, N. S. Polymer Solar Cells. In *Photoresponsive Polymers II*; Marder, S. R., Lee, K.-S., Eds.; Advances in Polymer Science; Springer: Berlin and Heidelberg, Germany, 2008; pp 1−86. (b) Zou, Y.; Gendron, D.; Neagu-Plesu, R.; Leclerc, M. *Macromolecules* **2009**, *42*, 6361.
(4) Winder, C.; Sariciftci, N. S. *J. Mater. Chem.* **2004**, *14*, 1077.
(5) Kim, J. Y.; Lee, K.; Coates, N.; Moses, D.; Nguyen, T. Q.; Dante, M.; Heeger, A. J. *Science* **2007**, *317*, 222.
(6) Park, S. H.; Roy, A.; Beaupre, S.; Cho, S.; Coates, N.; Moon, J. S.; Moses, D.; Lerclerc, M.; Lee, K.; Heeger, A. J. *Nat. Photonics* **2009**, *3*, 297.
(7) Ballauf, M.; Schmidt, G. F. *Mol. Cryst. Liq. Cryst.* **1987**, *147*, 163.

(8) McCulloch, I.; Heeney, M.; Chabinyc, M. L.; DeLongchamp, D.; Kline, R. J.; Cölle, M.; D. Warren, D.; Fischer, D.; D. Gundlach, D.; Hamadani, B.; Hamilton, R.; Richter, L.; Salleo, A.; Shkunov, M.; Sparrowe, D.; Tierny, S.; Zhang, W. *Adv. Mater.* **2009**, *21*, 1091.
(9) Carbonnier, B.; Egbe, D. A. M.; Birckner, E.; Grummt, U.-W.; Pakula, T. *Macromolecules* **2005**, *38*, 7546.
(10) Hoppe, H.; Sariciftci, N. S. *J. Mater. Chem.* **2006**, *16*, 45.
(11) Egbe, D. A. M.; Nguyen, L. H.; Schmidtke, K.; Wild, A.; Guenes, S.; Sieber, C.; Sariciftci, N. S. *J. Polym. Sci., Part. A: Polym. Chem.* **2007**, *45*, 1619.
(12) Weder, C.; Wrighton, M. S.; Spreiter, R.; Bosshard, C.; Günther, P. *J. Phys. Chem.* **1996**, *100*, 18931.
(13) Egbe, D. A. M.; Bader, C.; Nowotny, J.; Günther, W.; Klemm, E. *Macromolecules* **2003**, *36*, 5459.
(14) Wild, A.; Egbe, D. A. M.; Birckner, E.; Cimrova, V.; Baumann, R.; Grummt, U. W.; Schubert, U. S. *J. Polym. Sci., Part A: Polym. Chem.* **2009**, *47*, 2243.
(15) Hoppe, H.; Egbe, D. A. M.; Mühlbacher, D.; Sariciftci, N. S. *J. Mater. Chem.* **2004**, *14*, 3462.
(16) Hoppe, H.; Sariciftci, N. S.; Egbe, D. A. M.; Mühlbacher, D.; Koppe, M. *Mol. Cryst. Liq. Cryst.* **2005**, *426*, 255.
(17) Kietzke, T.; Shin, R. Y. C.; Egbe, D. A. M.; Chen, Z.-K.; Sellinger, A. *Macromolecules* **2007**, *40*, 4424.
(18) Kasai, N.; Kakudo, M. *X-ray diffraction by macromolecules*: Springer: Heidelberg, Germany, 2005.
(19) Milberg, M. E. *J. Polym. Sci., Part A* **1966**, *4*, 801.
(20) Milberg, M. E. *J. Appl. Phys.* **1962**, *5*, 1766.
(21) Egbe, D. A. M.; Türk, S.; Rathgeber, S.; Kühnlenz, F.; Jadhav, R.; Wild, A.; Birckner, E.; Getachew, A.; Pivrikas, A.; Cimrova, V.; Knör, G.; Sariciftci, N. S.; Hoppe, H. Submitted for publication.
(22) Egbe, D. A. M.; Carbonnier, B.; Birckner, E.; Grummt, U. W. *Prog. Polym. Sci.* **2009**, *34*, 1023.
(23) Granier, T.; Thomas, E. L.; Gagnon, D. R.; Karasz, F. E.; Lenz, R. W. *J. Polym. Sci: PartB* **1986**, *24*, 2793.
(24) Lee, J. L.; Pearce, E. M.; Kwei, T. K. *Macromolecules* **1997**, *30*, 6877.
(25) Tekin, E.; Wijlaars, H.; Holder, E.; Egbe, D. A. M.; Schubert, U. S. *J. Mater. Chem.* **2006**, *16*, 4294.